© 2022. Published by The Company of Biologists Ltd | Development (2022) 149, dev199615. doi:10.1242/dev.199615

TECHNIQUES AND RESOURCES

RESEARCH REPORT

FRaeppli: a multispectral imaging toolbox for cell tracing and dense tissue analysis in zebrafish

Sara Caviglia[1,2,‡,§], Iris A. Unterweger[1,‡], Akvilė Gasiūnaitė[1,*], Alexandre E. Vanoosthuyse[1], Francesco Cutrale[3,4], Le A. Trinh[3,5], Scott E. Fraser[3,4,5], Stephan C. F. Neuhauss[2] and Elke A. Ober[1,§]

ABSTRACT

Visualizing cell shapes and interactions of differentiating cells is instrumental for understanding organ development and repair. Across species, strategies for stochastic multicolour labelling have greatly facilitated *in vivo* cell tracking and mapping neuronal connectivity. Yet integrating multi-fluorophore information into the context of developing zebrafish tissues is challenging given their cytoplasmic localization and spectral incompatibility with common fluorescent markers. Inspired by *Drosophila* Raeppli, we developed FRaeppli (Fish-Raeppli) by expressing bright membrane- or nuclear-targeted fluorescent proteins for efficient cell shape analysis and tracking. High spatiotemporal activation flexibility is provided by the Gal4/UAS system together with Cre/lox and/or PhiC31 integrase. The distinct spectra of the FRaeppli fluorescent proteins allow simultaneous imaging with GFP and infrared subcellular reporters or tissue landmarks. We demonstrate the suitability of FRaeppli for live imaging of complex internal organs, such as the liver, and have tailored hyperspectral protocols for time-efficient acquisition. Combining FRaeppli with polarity markers revealed previously unknown canalicular topologies between differentiating hepatocytes, reminiscent of the mammalian liver, suggesting common developmental mechanisms. The multispectral FRaeppli toolbox thus enables the comprehensive analysis of intricate cellular morphologies, topologies and lineages at single-cell resolution in zebrafish.

KEY WORDS: PhiC31 integrase, Canaliculi topology, Cell shape, Liver, Multicolour cell labelling, Zebrafish

INTRODUCTION

A prerequisite for uncovering the cellular architecture of organs and entire embryos, as well as the intricate cellular processes that guide tissue formation, such as cell interaction, movement and proliferation, is the capability to visualize the resident cell types at single-cell resolution (Megason and Fraser, 2007). The transparency and rapid growth of zebrafish are ideal for dissecting the cellular processes that establish tissue architectures in vertebrate development and disease. Uniform membrane labelling within a tissue generates an approximate view of cellular shapes, suitable for uniformly shaped cells, while elaborate cellular morphologies and intricate contacts, e.g. via protrusions (Caviglia and Ober, 2018), remain elusive. Instead, sparse labelling by expression of a single membrane-targeted fluorescent protein (FP) (e.g. Cayuso et al., 2016; Sanders et al., 2013) outlines individual cells and has significantly advanced our understanding of dynamic cell behaviours. Nevertheless, information concerning the cellular topologies, the nature and morphology of contacts between adjacent cells is frequently lacking, because the cellular microenvironment remains unlabelled.

The need to distinguish neighbouring cells has been met partially by the Brainbow system (Livet et al., 2007), which randomly labels neighbouring cells by the stochastic expression of three or four FPs (reviewed by Richier and Salecker, 2015; Weissman and Pan, 2015). Stochastic combinatorial expression of spectrally distinct FPs is achieved by their sequential arrangement in a DNA cassette, with each FP flanked by recombinase recognition sites, permitting stochastic recombinase-mediated DNA excision or inversion. This approach, pioneered in mice, has been adapted in a variety of species, including zebrafish (Gupta and Poss, 2012; Livet et al., 2007; Pan et al., 2013; Richier and Salecker, 2015; Weissman and Pan, 2015). Key advances range from uncovering distinct neural networks (e.g. Fontenas and Kucenas, 2021; Forster et al., 2017) to clonal dominance of stem cell-like populations in differentiating tissues (e.g. (Gupta and Poss, 2012; Gurevich et al., 2016). Brainbow-tools targeting FPs to specific cellular compartments, such as the membrane, have been successfully used in mice and flies, but rarely in zebrafish (Chan et al., 2022; Forster et al., 2017). Moreover, comprehensively resolving the complex organization of tissues requires information about specific cell types, subcellular structures (e.g. cytoskeleton) or signalling pathway activity as landmarks, which could be achieved by combining multicolour cell labelling systems with spectrally distinct signals, such as infrared proteins (Cook et al., 2019). However, the majority of currently available reporter lines express GFP, which overlaps with the spectra of existing Brainbow-like systems and thereby precludes their combined use.

To address those experimental needs, we introduce the FRaeppli (Fish-Raeppli) tools: transgenic lines inspired by Raeppli, a whole-tissue labelling system developed in *Drosophila* (Kanca et al., 2014). FRaeppli expresses four bright monomeric FPs – mOrange2, mKate2, mTFP1 and TagBFP – that are spectrally distinct from GFP and infrared fluorophores, allowing simultaneous acquisition of six distinct labels. We demonstrate the versatility of the membrane-tethered *fraeppli-caax* for large-scale visualization

[1]University of Copenhagen, NNF Center for Stem Cell Biology (DanStem), Blegdamsvej 3B, 2200 Copenhagen N, Denmark. [2]University of Zurich, Department of Molecular and Life Sciences, Winterthurerstrasse 190, 8057 Zürich, Switzerland. [3]Translational Imaging Center, University of Southern California, 1002 West Childs Way, Los Angeles, CA 90089, USA. [4]Biomedical Engineering, University of Southern California, 1002 West Childs Way, Los Angeles, CA 90089, USA. [5]Molecular and Computational Biology, University of Southern California, 1002 West Childs Way, Los Angeles, CA 90089, USA.
*Present address: Technische Universität Dresden, Center for Molecular and Cellular Bioengineering (CMCB), Center for Regenerative Therapies Dresden (CRTD), Fetscherstrasse 105, 01307 Dresden, Germany.
‡These authors contributed equally to this work

§Author for correspondence (sara.caviglia@mls.uzh.ch, elke.ober@sund.ku.dk)

S.C., 0000-0001-9832-2566; I.A.U., 0000-0001-7041-8638; A.G., 0000-0003-2943-9896; F.C., 0000-0003-0517-3069; L.A.T., 0000-0001-7965-8769; S.E.F., 0000-0002-5377-0223; S.C.F.N., 0000-0002-9615-480X; E.A.O., 0000-0002-5195-1012

Handling Editor: Steve Wilson
Received 21 January 2022; Accepted 20 July 2022

Development (2022) 149, dev199615. doi:10.1242/dev.199615

of cell topologies and the nuclear *fraeppli-nls* for lineage tracing analysis in dense tissues. We show its versatility with examples of larval and adult tissues, genetic strategies to control clone size, live imaging and a hyperspectral protocol for time-efficient data acquisition.

RESULTS AND DISCUSSION

Design and general expression characteristics of FRaeppli

For a versatile next-generation multicolour cell labelling system in zebrafish, we adapted *Drosophila* Raeppli (Kanca et al., 2014) and produced F(ish)Raeppli. The colour-cassette consists of four bright FPs: mOrange2 (E2-Orange in *fraeppli-nls*), mKate2, mTFP1 and TagBFP (Fig. 1A, Fig. S1). Based on their excitation and emission spectra, imaging of these FPs can be performed with fluorophores in the green/GFP and far-red range. FRaeppli is therefore compatible with many transgenic lines and diverse cell and organelle labels. We generated two different versions for application-specific use: in *fraeppli-nls*, a nuclear localization signal targets the FPs to the nucleus (NLS; Fig. 1B,C) enabling cell lineage and growth analyses; in *fraeppli-caax*, a Ras farnesylation sequence (CAAX)

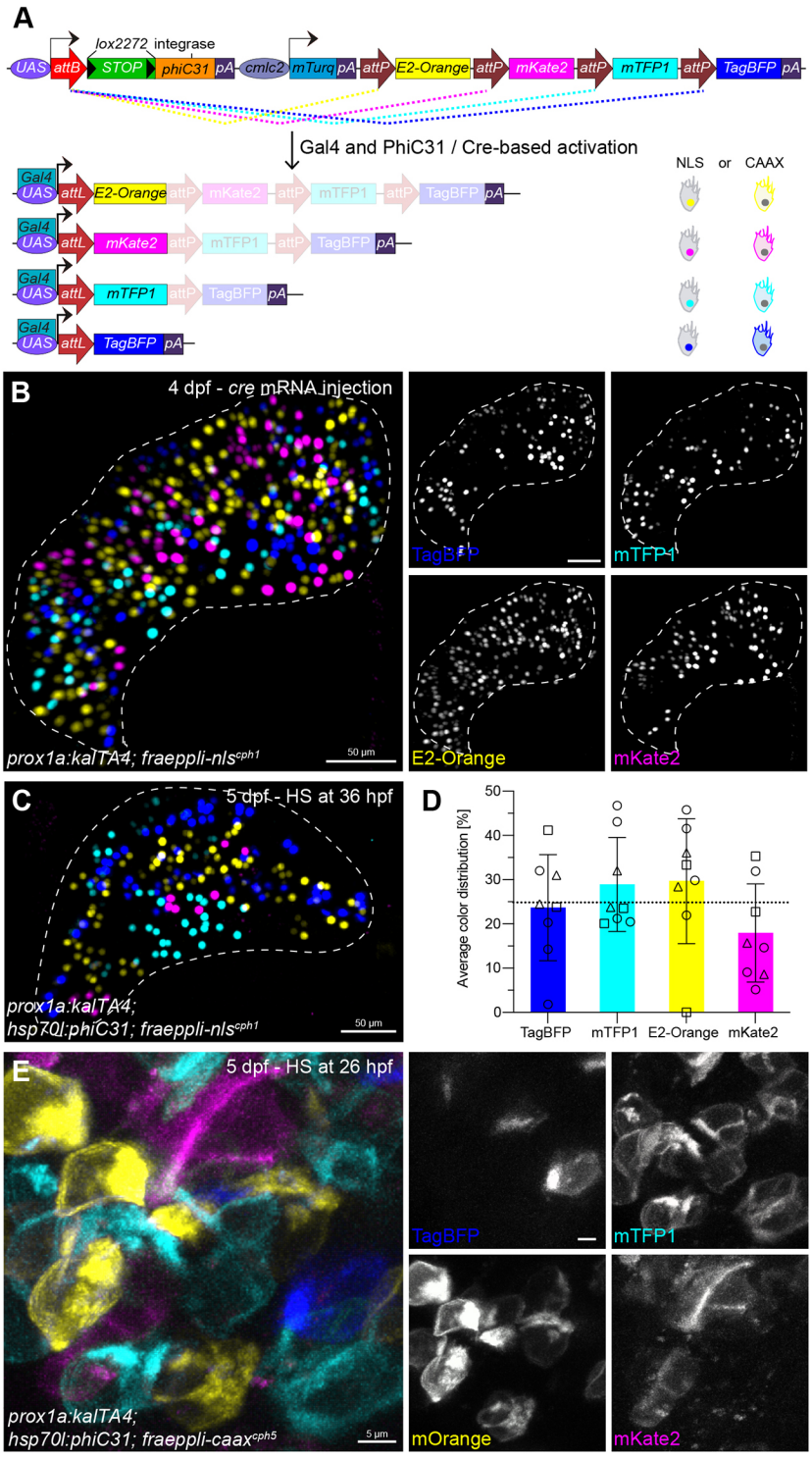

Fig. 1. FRaeppli expression is controlled by sequential Gal4 and Cre/PhiC31 activity. (A) Schematic of FRaeppli activation. Cre excises a stop cassette, priming FRaeppli for activation. Gal4/UAS initiates *phiC31* expression, which drives *attB* and *attP* recombination, and stochastic expression of one fluorescent protein (FP). FPs are targeted to the cell membrane in *fraeppli-caax* or to the nucleus in *fraeppli-nls*. The FP order represents *fraeppli-nls*; in *fraeppli-caax*, it is mKate2-mTFP1-mOrange2-TagBFP (Fig. S3E). (B,C) Activation of *fraeppli-nls; prox1a:kalTA4* by *cre* mRNA injection (B) or by *hsp70l:phiC31* (C) generates nuclear clusters in four colours (*N*=3 experiments, *n*≥8 embryos). (D) Quantification of the *fraeppli-nls* colour selection frequency; *N*=3 experiments, *n*=8 embryos. Data are mean±s.d. (unpaired two-tailed *t*-test). (E) Activation of *fraeppli-caax;prox1a:kalTA4* with *hsp70l: phiC31* outlines individual cell clusters with all colours (*N*=2 experiments, *n*=5 embryos). In all FRaeppli-CAAX images, the gamma-value was set to 1.2-1.5 to highlight darker regions of cell membranes. Scale bars: 50 µm in B,C; 5 µm in E.

Development (2022) 149, dev199615. doi:10.1242/dev.199615

directs the FPs to the cell membrane for cell shape analyses (Fig. 1E). Recombination of the colour-cassette is mediated by the bacteriophage PhiC31 integrase (Bischof et al., 2007; Lister, 2011; Thorpe et al., 2000), only thus far used for transgenesis in zebrafish (Hu et al., 2011; Mosimann et al., 2013). PhiC31 catalyses recombination of unidirectional *attB* and *attP* sites, excising DNA fragments flanked by these sites. In FRaeppli, a single *attB* site is placed directly after the promoter and *attP* sites before each of the FP open reading frames (Fig. 1A). Recombination events generate *attL* sites, incompatible with further PhiC31-mediated recombination and thereby initiating stable expression of one FP per cell (Fig. S1). PhiC31 is built into the FRaeppli cassette and controlled by an upstream 1.5 kb-STOP-cassette flanked by *lox2272* sites. Cre-mediated recombination of these sites excises the STOP-cassette, placing *phiC31* expression under direct control of an upstream activating sequence (UAS). Expression of the FRaeppli construct is driven by the binary Gal4/UAS system (Brand and Perrimon, 1993). Binding of the transcriptional activator Gal4 or optimized versions (Distel et al., 2009) to regulatory *UAS* elements drives transcription of both PhiC31 and the stochastically selected FP, following PhiC31-mediated *attB/attP* recombination (Fig. S1D).

We tested FRaeppli recombination in the forming liver first by injecting *cre* mRNA into stable transgenic *fraeppli-nls* or *fraeppli-caax* embryos at the one-cell stage, labelling cells in four colours in most embryos (Fig. 1B, Fig. S2A). This indicates the correct expression of the FRaeppli-inbuilt *phiC31* and subsequent induction of all four recombination events. Next, we tested recombination after conditional Cre expression by crossing *fabp10a:kalTA4;fraeppli-caax* to *hsp70l:cre* and subjecting embryos to a heat-shock at 33 h post-fertilisation (hpf). They expressed all four FPs in the liver (Fig. S2B,C), indicating that all elements of FRaeppli work correctly. Three independent lines each of *fraeppli-nls* and *fraeppli-caax* were identified, *fraeppli-nls*^{cph1}, *fraeppli-nls*^{cph2}, *fraeppli-nls*^{cph3}, *fraeppli-caax*^{cph4}, *fraeppli-caax*^{cph5} and *fraeppli-caax*^{cph6}, with different levels of transgene activation (Fig. S2A-E). Most experiments were performed with the most penetrant lines: *fraeppli-nls*^{cph1}, *fraeppli-nls*^{cph2}, *fraeppli-nls*^{cph3} and *fraeppli-caax*^{cph4}.

We expanded the conditional strategies for FRaeppli labelling by generating an inducible transgenic PhiC31 line: *hsp70l:phiC31*^{cph7}. Activation is faster, as it bypasses Cre-induced excision of the STOP-cassette by directly triggering colour-cassette recombination and is therefore more suitable for early embryogenesis (Fig. S1C). Similar to the FRaeppli-inbuilt PhiC31, exogenous PhiC31 expression in *prox1a:kalTA4;hsp70l:phi;fraeppli-nls* or *fraeppli-caax* larvae efficiently induces all recombination events (Fig. 1C,E). Examining mRNA and protein expression over time, by *in situ hybridization* chain reaction (HCR) and *hsp70l:phiC31-sfGFP-NLS* expression, respectively, showed increasing expression of *phiC31* mRNA between 2 and 4 h and of PhiC31 protein 4 h post heat-shock (Fig. S3A-C; Movie 1). Direct induction of FRaeppli colour recombination by PhiC31 allows subsequent independent Cre-mediated gene inactivation, which was impossible with previous Cre-controlled multicolour tools.

Unbiased colour selection ensures differential labelling of neighbouring cells. We therefore assessed colour representation using different transgene activation strategies and determined no significant colour bias in *fraeppli-nls* or *fraeppli-caax* (Fig. 1D, Fig. S2E). Nonetheless, we noticed that the timely appearance of the FPs can vary, mostly starting with tagBFP-CAAX or tagBFP-NLS (Fig. S3D,H), followed by the other FPs and mKate2-CAAX or E2-Orange-NLS appearing last. Depending on the experimental context, the lag time between the first and last FP can take between 4 and 30 h. To exclude asynchronous PhiC31-mediated recombination as the underlying reason, we assessed recombination of the colour-cassette at the genomic level (Fig. S3E-G) by performing PCR amplification at 10 and 24 hpf in single *hsp70l:gal4;fraeppli-caax* embryos injected with *phiC31* mRNA. This showed successful recombination of all four FP loci in individual embryos at 10 hpf (Fig. S3F-F″′), indicating synchronized recombination during blastula stages. Likewise, *cre* mRNA-injected embryos of the same genotype show efficient amplification of all recombined FP loci 24 h after heat-shock, indicating that FRaeppli-inbuilt PhiC31 can also drive synchronous recombination of all FP loci (Fig. S3G). Delayed FP appearance is likely due to a combination of individual FP maturation times, e.g. 13 min for tagBFP versus 78 min for E2-Orange (www.fpbase.org) and mRNA stability issues given the colour-cassette contains a single polyA, after tagBFP. The farther the respective FP is from the polyA, the longer it takes to build up detectable FP protein levels. Furthermore, the strength of a given Gal4 driver influences the temporal gap between recombination and colour detection. In the liver, it can take 11 or 30 h for all FRaeppli FPs to appear, after stimulating recombination using *fabp10a:kalTA4* or *prox1a:kalTA4*, respectively. Conversely, using a strong ubiquitous Gal4-driver during gastrulation stages can drive the appearance of all colours between 9 and 13 hpf, making it suitable for the study of early developmental processes (Fig. S3H). The strength of the Gal4 driver is therefore an important consideration for experimental design. These results corroborate that FRaeppli lines stochastically label cells by simultaneous recombination events, which is pivotal for tissue morphology and lineage-tracing studies.

Temporal and spatial activation of FRaeppli cell labelling

A key feature of multicolour cell labelling is the versatile control of recombination in space and time, to mark progenitor cells before the onset of differentiation for lineage tracing, or to label individual cells for high-resolution cell morphology and cell interaction studies. Different PhiC31, Cre and Gal4 expression methods were assessed for labelling density by temporally controlling FRaeppli recombination in the liver (Fig. 2G). Dense labelling can be achieved by *phiC31* mRNA injection mediating recombination during blastula stages and *prox1a:kalTA4*-induced FP expression in liver progenitors (Fig. 2A). Labelling density is slightly reduced when *cre* mRNA injection removes the STOP cassette and *prox1a:kalTA4* controls recombination by subsequent expression of the FRaeppli-inbuilt PhiC31 (Fig. 2B). Late induction of recombination by *hsp70l:cre* at 70 hpf results in lower labelling density (Fig. 2C). Similar activation strategies lead to progressively reduced labelling using the hepatocyte driver *fabp10a:kalTA4*, which is activated 1-1.5 days later, led to progressively reduced labelling (Fig. 2D-F), demonstrating that diverse tissue-specific drivers can control both FRaeppli recombination and expression at different developmental stages.

To validate FRaeppli for broad embryo labelling, we employed the ubiquitous driver *hsp70l:gal4* and *phiC31* or *cre* mRNA injection in *fraeppli-caax* embryos. Initiating recombination at different time-points between 26 and 72 hpf, labels cells at different densities (Fig. 2H-K, Fig. S2G-I), without apparent tissue bias.

Altogether, the combination of the Gal4/UAS and Cre/lox systems opens up the possibility of selecting a subset of cells within a population by using two different promoters. For example, this is achieved by intersecting a tissue-wide Gal4 driver with a cell type-specific Cre- or CreERT2 line, or vice versa. This dual activation

Development (2022) 149, dev199615. doi:10.1242/dev.199615

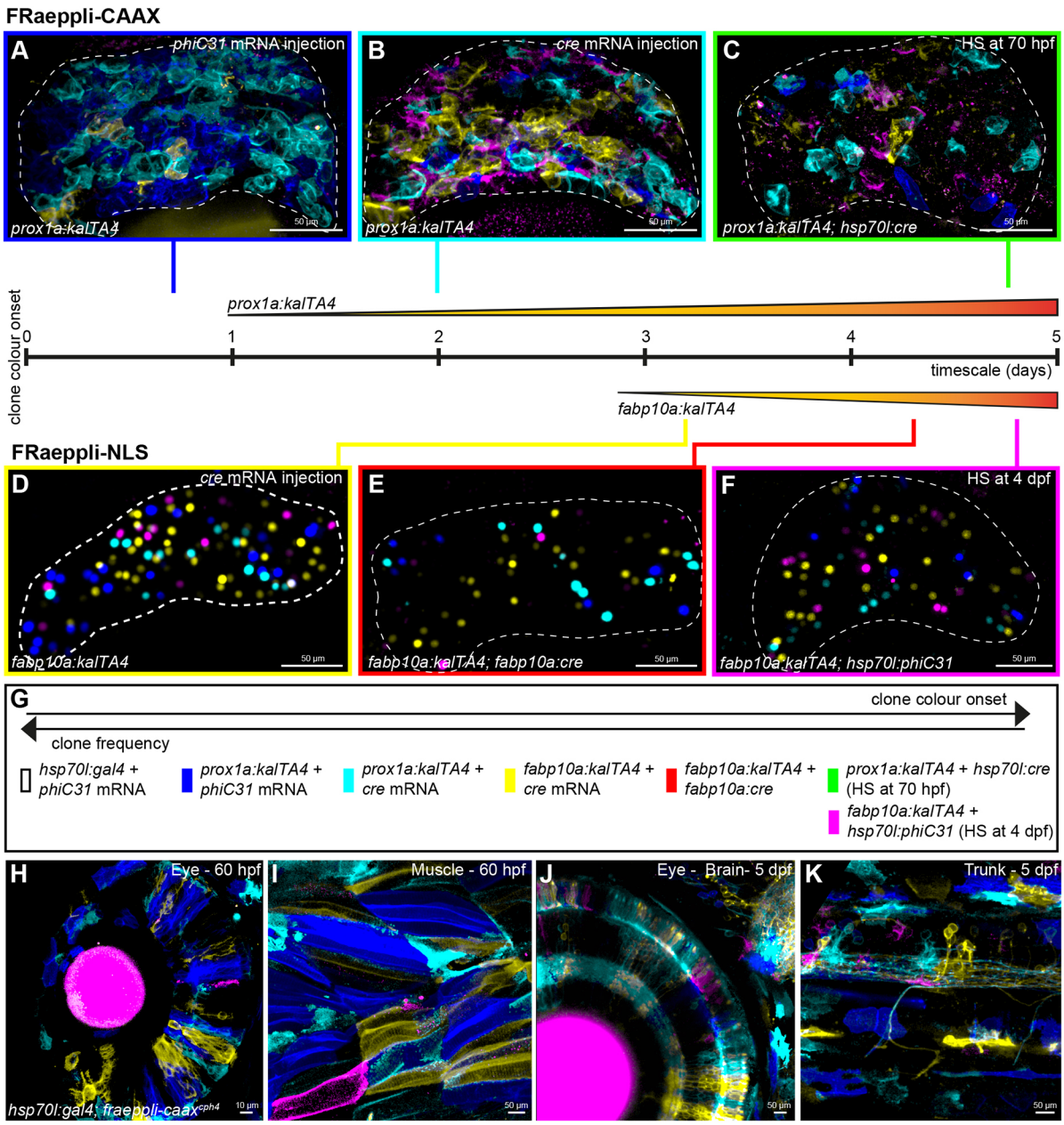

Fig. 2. Versatility of spatiotemporal FRaeppli activation. (A,B,D) Initiating FRaeppli recombination by *phiC31* mRNA injection (A) produces denser cell labelling than with *cre* mRNA injection (B,D). (C,E,F) Late activation with inducible (C) or cell-type specific (E,F) transgenic *cre* lines marks fewer cells. (G) Onset of Gal4 driver expression influences the temporal appearance of fluorescence (A-G; $N \geq 2$ experiments, $n \geq 8$ embryos). (H-K) Widespread FRaeppli-CAAX expression in tissues throughout the embryo, following injections with *phiC31* (H,I) or *cre* mRNA (J,K). Transgene expression was maximized by daily heat-shocks starting at 26 hpf. 60 hpf (H,I; $n=6$ embryos) and 5 dpf (J,K; $N=2$ experiments, $n=9$ embryos) larvae are shown.

strategy enables the analysis of new subpopulations arising from genome-wide transcriptome studies by visualizing cell shapes, behaviours and lineages at single-cell resolution. Thus, FRaeppli is a highly versatile cell-labelling system, as multiple approaches allow to control temporal and broad or tissue-specific multicolour expression, achieved by strategic combination of Gal4/UAS, Cre/lox and PhiC31 systems.

Advanced image acquisition and cell labelling strategies for FRaeppli

One challenge for imaging multispectral cell labelling is the frequently overlapping excitation and emission spectra of the used fluorophores (Cutrale et al., 2017), which is usually addressed by sequential imaging (Kanca et al., 2014; Fig. S4A). However, imaging time increases concomitantly with colour number (Fig. S4B). Alternatively, simultaneous excitation and acquisition of all channels by spectral imaging reduces imaging time (Dickinson et al., 2001). To test the feasibility, we first acquired all spectral data of larval *prox1a:kalTA4;fraeppli-nls* livers by lambda scanning (Fig. 3A), using 32 channels collecting signal from the 410-694 nm range, effectively reducing imaging time by 50-75%. Second, we employed the Hyper-Spectral Phasor software (HySP), which transforms the acquired spectral information by Fourier transformation into a 2D PhasorPlot, (Fig. 3A′) for subsequent label-unmixing (Fig. 3A″; Cutrale et al., 2017). This powerful method allows fast unmixing of large spectral images without calibration

Development (2022) 149, dev199615. doi:10.1242/dev.199615

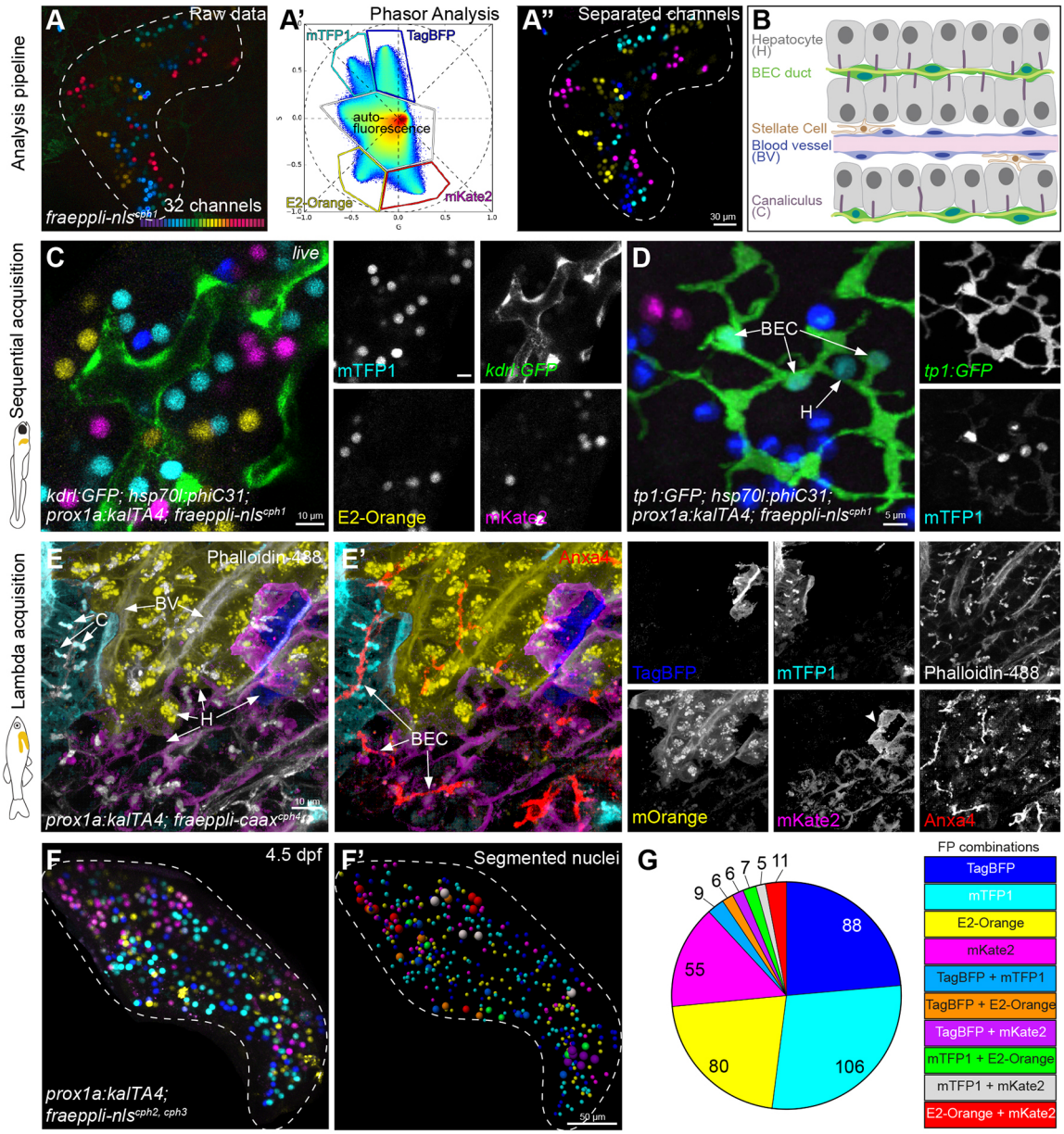

Fig. 3. Advanced strategies for FRaeppli acquisition and multiplexed tissue labelling. (A-A″) Spectral imaging of FRaeppli (A) can be unmixed by HySP (A′) into four channels (A″; *N*=2 experiments, *n*=10 embryos). (B) Schematic showing the functional zebrafish liver architecture. (C,D) FRaeppli+1 label: (C) live imaging of 5 dpf liver co-expressing hepatic FRaeppli-NLS and endothelial *kdrl:GFP* (*n*=3); (D) fixed 4.5 dpf liver co-expressing hepatic FRaeppli-NLS and *tp1:GFP* in biliary epithelial cells (BECs) and hepatocytes (H) (*N*=3 experiments, *n*=11 embryos). (E,E′) FRaeppli+2 labels: spectral acquisition of 1-year-old adult liver stained using phalloidin (green) outlining liver architecture (E) and for Anxa4 (red) to visualize BEC ducts (E′) (*N*=2 experiments). (F) A combination of two *fraeppli-nls* transgenes generates clones expressing up to ten discernible hues in 5 dpf liver (*N*=2 experiments, *n*=3 embryos). (F′) Nuclei were segmented and pseudo-coloured; nuclei expressing two different FPs have a larger diameter that facilitates visualization. (G) Absolute colour combination frequencies in the liver. Scale bars: 30 µm in A; 10 µm in C-E; 50 µm in F.

using reference samples for each spectral signature. Directly comparing the same *prox1a:kalTA4;fraeppli-nls* liver acquired sequentially with band pass filters (Fig. S4D) or spectrally (Fig. S4E) showed that hyperspectral imaging combined with HySP processing enables additional spectral separation of autofluorescence-derived noise (Cutrale et al., 2017), which is advantageous for metabolically active tissues like the liver. This method is suitable for live and fixed tissues of *fraeppli* larvae and adults (Fig. 3D, Fig. S4C,E).

Adding cellular and subcellular markers to FRaeppli-labelled populations would significantly extend the experimental possibilities for morphology and lineage studies. Hence, we tested the compatibility of FRaeppli with subpopulation-specific cell labels. First, we combined *fraeppli-nls* with the endothelial *kdrl:GFP* line, showing live how labelled hepatic cells arrange along the blood vessel network and the clear spectral separation of all labels, including GFP (Fig. 3C). Furthermore, inducing *hsp70l:*phiC31-mediated *fraeppli-nls* recombination in liver progenitors before lineage decision produced clones of diverse fates, containing *tp1:GFP*-positive biliary cells and *tp1:GFP*-negative hepatocytes, showcasing the advantage of FRaeppli for lineage-tracing studies involving GFP reporters (Fig. 3D).

Development (2022) 149, dev199615. doi:10.1242/dev.199615

Next, we visualized the liver architecture (Fig. 3B) by staining *fraeppli-caax* and *fraeppli-nls* adult liver sections and larval livers for actin and Anxa4 or TO-PRO, highlighting the hepatocyte canaliculi, blood vessel network and biliary network or nuclei, respectively (Fig. 3E-E′, Fig. S5A-B′). These applications demonstrate the compatibility of FRaeppli with at least two spectrally distinct labels, highlighting features on a tissue, cellular and subcellular scale. Notably, FRaeppli expression, depending on the Gal4-driver, is not only stably maintained into adulthood, but is also compatible with SeeDB2 clearing (Ke et al., 2016; Fig. S5A; Movie 2), permitting long-term clonal analysis.

Moreover, inducing colour recombination in embryos carrying multiple transgene copies would increase the number of distinct colour hues for differential cell labelling. Crossing two *fraeppli-nls* alleles lead to up to ten colours in the developing liver (Fig. 3F,F′), indicating successful recombination of all possible combinations, with comparable cell numbers expressing two distinct FPs (Fig. 3G). Altogether, we established the compatibility of FRaeppli with hyperspectral imaging and analysis strategies, with tissue-clearing approaches, and with common GFP and infrared tools that significantly expand experimental possibilities for high-resolution multicolour morphological and functional studies.

Deciphering complex tissue organization: using FRaeppli to study hepatocyte polarity and interactions in the zebrafish liver

A powerful advantage of FRaeppli-CAAX is the ability to differentially label the morphologies of adjacent cells in order to untangle complex cellular interactions. Using this approach, we investigated zebrafish liver architecture and its similarity with that of mammals. Previous studies have reported that canaliculi, the apical membrane of hepatocytes, exhibit an intracellular topology by forming tube-like membrane invaginations within single hepatocytes (Figs 3B and 4A; Lorent et al., 2004; Sakaguchi et al., 2008). In mammals, the apical tubules are lined by membranes of adjacent cells, thus displaying intercellular shared topologies (Fig. 4A; Treyer and Musch, 2013). However, canalicular topologies in the zebrafish liver have not been assessed at single-cell resolution. We therefore stained *fabp10a:kalTA4;fraeppli-caax* larvae injected with *cre* mRNA using a multidrug resistance protein 1 (Mdr1) antibody, which marks mature canalicular membrane at 5 days post fertilisation (dpf). Combining commercial and custom-made image analysis tools (see Materials and Methods), we developed an analysis pipeline to quantify canalicular topologies (Movie 3). This revealed, in addition to the known intracellular canaliculi (Fig. 4A,B), a substantial proportion of intercellular canaliculi, shared between the membranes of neighbouring hepatocytes (Fig. 4A,C,D; Movie 3), demonstrating plasticity of canalicular topology in zebrafish. Altered canalicular topologies are also observed upon chronic liver injury in mammals (Clerbaux et al., 2019; Kamimoto et al., 2020), further suggesting that canaliculi topology is generally more plastic than previously known and that common mechanisms of canaliculi formation exist between zebrafish and mammals.

Live imaging is instrumental for elucidating morphodynamic cell behaviours driving embryonic development. Following several independent clones in the same organ enables investigation of cell rearrangement and interactions during tissue formation. Sparse labelling with a single membrane-localised FP has shown that directional progenitor migration determines liver position (Cayuso et al., 2016). Yet it is unknown to what extent cells rearrange as the organ differentiates. We monitored hepatocyte behaviours as the liver develops its functional organisation by time-lapse imaging in *prox1a:kalTA4;fraeppli-caax* embryos injected with *phiC31* mRNA (Movie 4). Simultaneous tracking of individual cell clusters over time showed continuous changes of cluster morphologies and interactions, including protrusive activity evident at cluster edges, that indicate dynamic cell rearrangement during hepatic differentiation (Fig. 4E-F′). Tracing cluster dynamics showed diverse behaviours, including intermingling of adjacent clusters that led to fragmentation (Fig. 4E′; Movie 4). Cluster merging can occur in parallel, when detached cells contact other clusters and fuse (Fig. 4E″,F′). Combining real-time imaging with multicolour FRaeppli labelling revealed that differentiating hepatocytes are unexpectedly dynamic, which is essential information for understanding the establishment of tissue architecture and organ growth (Rulands and Simons, 2016). It further highlights the suitability of FRaeppli for collecting time series of dense tissues at subcellular resolution, including those of internal organs. The presented FRaeppli applications not only generate valuable insights into how complex tissues like the liver form but also allude to the extended experimental possibilities that the tools offer.

In summary, the FRaeppli toolbox offers a new cell labelling system that is: (1) targeting FPs to cell membranes and nuclei required for deciphering intricate cell behaviours and efficient lineage tracing; (2) spectrally compatible with many existing transgenic reporter lines and cell labels; and (3) amenable to sequential PhiC31-based cell labelling and conditional Cre/lox gene inactivation. Together with the growing number of conditional Cre-based gene inactivation tools (Carney and Mosimann, 2018) FRaeppli will enable connecting cell morphologies with gene function, which is the essential next step for understanding how tissues are built. The experimental versatility of FRaeppli thereby opens up powerful new applications for analyses of cellular behaviours in dense multicellular tissues.

MATERIALS AND METHODS

Zebrafish husbandry

Zebrafish (*Danio rerio*) embryos and adults were kept according to standard laboratory conditions (Westerfield, 2000). Research was performed in accordance with ethical guidelines approved by the Danish Animal Experiments Inspectorate (Dyreforsøgstilsynet). The following transgenic lines were used: *tgBAC(prox1a:kalTA4)*^{uq3bh} (Koltowska et al., 2015), *tg(hsp70l:gal4)*^{fci1} (Cayuso et al., 2016), *tg(kdrl:EGFP)*^{s843} (Jin et al., 2005), *tg(hsp70l:cre)*^{zdf13} (Feng et al., 2007), *tg(-2.8fabp10a:Cre,cryaa:Venus)*^{s955} (Ni et al., 2012) and *tg(tp1-MmHbb:EGFP)*^{um14} (Parsons et al., 2009).

Constructs

fraeppli-nls and *fraeppli-caax*

NLS- and CAAX-tagged fluorescent proteins from *Drosophila* Raeppli were combined into a final pBlueScript (pBS) vector following the original strategy described by Kanca et al. (2014). The order of FPs differs in the two FRaeppli cassettes: the *pBS-FP-CAAX* cassette contains mKate2-mTFP1-mOrange2-TagBFP, whereas *pBS-FP-NLS* cassette contains E2-Orange-mKate2-mTFP1-TagBFP. A fragment containing the SV40pA was amplified with primers 334 and 335 from the original pCS2+ vector (Rupp et al., 1994). The amplicon was cut with XbaI/SpeI and ligated into *pBS-FP-CAAX* cassette and *pBS-FP-NLS* cassette, both linearized with SpeI. A fragment containing the UAS promoter was amplified using primers 332 and 333 from *UAS:ephrinb1* (Cayuso et al., 2016) and cloned into pJET1.2 (Thermo Fisher Scientific). A cassette containing a minimal *attB* site, an *H2B-NeonGreen-STOP* coding sequence flanked by two *Lox2272* sites and several unique restriction sites for subsequent cloning steps (called

Development (2022) 149, dev199615. doi:10.1242/dev.199615

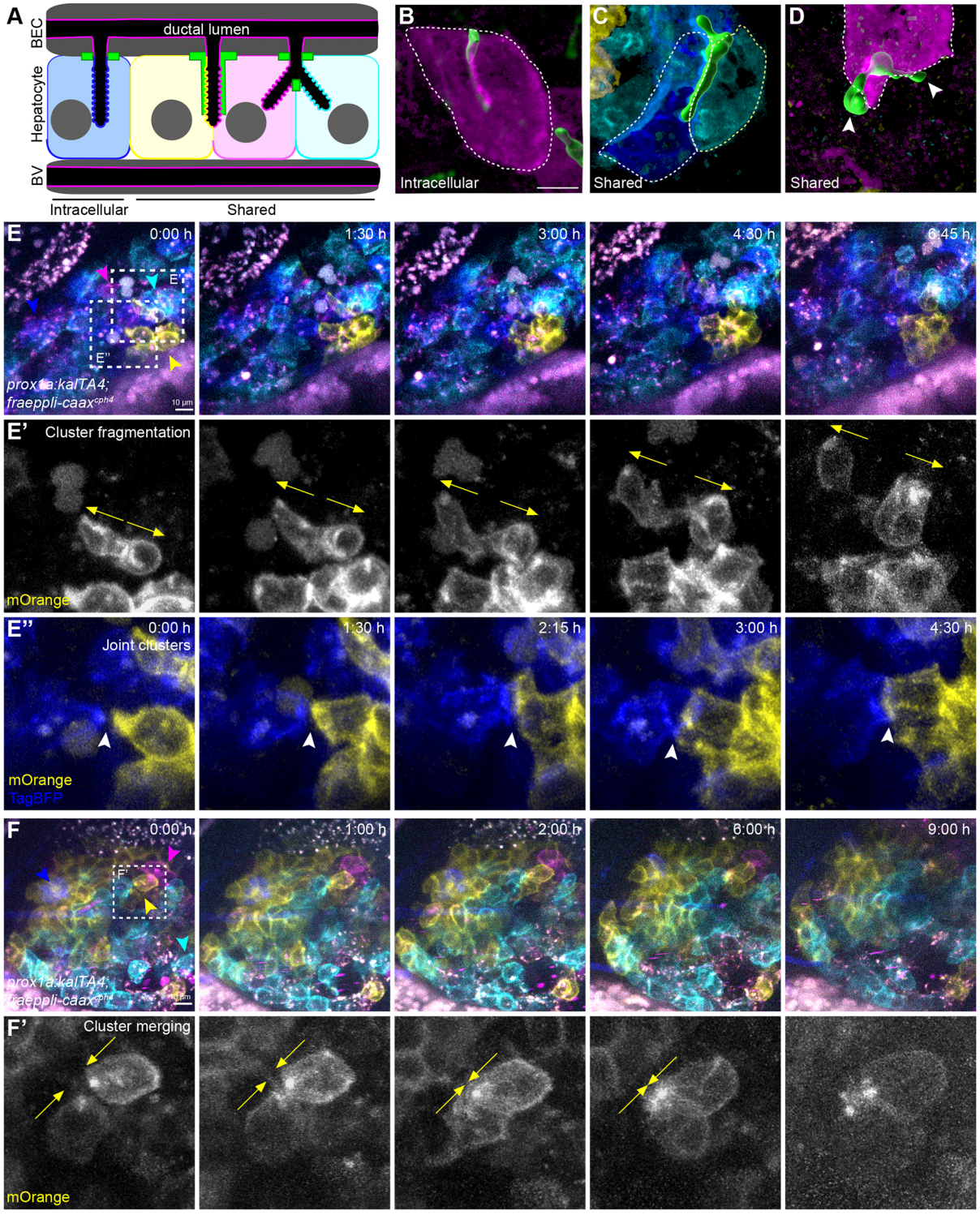

Fig. 4. Topological analysis and long-term imaging of hepatocyte clones. (A) Schematic depicting intracellular and shared canalicular topologies. (B-D) Examples of canalicular topologies at 5 dpf scored by semi-automatic classification of FRaeppli-CAAX-expressing hepatocytes, stained for canalicular protein Mdr1; arrowheads highlight canaliculi ends projecting into unlabelled hepatocytes (Movie 3; *N*=2 experiments; *n*=5 embryos). (E-F′) Live imaging of 72 hpf *fraeppli-caax* embryos using sequential acquisition at 12-15 min intervals. Tracing dynamic cell rearrangement in the liver reveals cells from the same cluster moving apart (E′, arrows) or separated cells merging and forming new contacts (E″,F′; arrows indicate the direction of movement; arrowheads indicate a growing contact; *N*=3 experiments; *n*=10 embryos). The areas magnified in E′, E″ and F′ are outlined in E,F. Scale bars: 5 µm in B-D; 10 µm in E,F.

ALNG) was synthesized as GeneBlock (IDT) and cloned using XbaI/NcoI into pJET-UAS cut with the same enzymes.

The H2B-NeonGreen contained in the *Lox2272*-flanked cassette, which was supposed to be expressed in unrecombined cells, and was subsequently replaced with standard GFP amplified with primers 371 and 372, and cloned in the ALNG cassette by AscI/NdeI, given the suspected toxicity of NeonGreen in zebrafish. Unfortunately, neither version was expressed, probably owing to the distance from the UAS.

Development (2022) 149, dev199615. doi:10.1242/dev.199615

The *phiC31 integrase* sequence followed by the *BGH polyadenylation* (pA) sequence was amplified with primers #51-340 from *pCDNA-phiC31-BGHpA* (Bischof et al., 2007), where a small sequence in the multiple cloning site was removed by XbaI/XhoI restriction and filled by Klenow DNA pol I (NEB). The full *phiC31 integrase* CDS was cloned after the ALGN cassette of *pJET-UAS-ALNG* using NsiI/BsrGI. The *cmlc2:mTurquoise* marker cassette was amplified from *UAS-self-cmlc2:mTurquoise* (derived from *pGEMT-cmlc2:mTurquoise*, a kind gift from J. Goedhart, University of Amsterdam, The Netherlands) with primers 267 and 353, and inserted in pJET. This plasmid was linearized with NheI and the cassette containing *UAS-ALGN-phiC31* integrase was cloned into it after release with AvrII/SpeI.

The resulting *pJET-UAS-ALGN-phiC31-cmlc2:mTurquoise* was used in subsequent steps to derive the final FRaeppli 1.0, which unfortunately could not be employed for the generation of transgenic lines, as the plasmid had already recombined in bacterial cells due to bacterial activation of the *UAS* promoter, followed by the unanticipated expression of the integrase.

To generate an intact FRaeppli 2.0 plasmid, refractory to recombination in bacterial cells, an intron from SV40 (Reddy et al., 1979) was placed at position 546 of the *phiC31* integrase-coding sequence, leading to a premature stop codon, which blocks the translation of a functional integrase only in bacterial cells. In eukaryotic cells, the intron is spliced out; therefore, a functional integrase can be generated upon *UAS* activation. A cassette containing the second *lox2272* site, the first part of *phiC31* integrase, the *SV40* intron and linkers needed for subsequent cloning steps were synthesized as a GeneBlock (IDT) and subcloned into pJET-*fraeppli2.0*. Subsequently, the NdeI/BstEII fragment of pJET-*fraeppli2.0* cloned into *pJET-UAS-ALNG-phiC31-cmlc2:mTurquoise* also cut with the same enzymes was introduced into the SV40 intron in the integrase CDS. The resulting plasmid was then cut with NotI and the fragment (*UAS-ALGN-phiC31-intron-cmlc2:mTurquoise*) cloned into *pBS-FP-CAAX* cassette and *pBS-FP-NLS* cassette. The *miniTol2* sequences (Urasaki et al., 2006), taken from *UAS-self- cmlc2:mTurquoise* were inserted in the resulting pBS vectors by substitution of the XhoI-bound fragment, generating the final FRaeppli2.0-NLS and FRaeppli2.0-CAAX, which were used for transgenesis. All primers used in this study are listed in Table S1.

fabp10a:kalTA4;cryaa:Venus

The optimized Gal4 activator *kalTA4*-coding sequence (Distel et al., 2009) was inserted after the *fabp10a* promoter (Her et al., 2003) into the *I-SceI-fabp10a:cre-cryaa:Venus* plasmid (Feng et al., 2007), where *cre* was removed with ClaI/NotI. An unnecessary *polyA* sequence was then removed by cutting with XbaI. The final plasmid was sequenced with primers 327 and 331.

hsp70l:phiC31

The EcoRI/NheI *phiC31-integrase-BGHpA* fragment was sub-cloned from the *UAS:phiC31-cryaa:Citrine* plasmid (this work) into the I-SceI-containing backbone of the *fabp10a:kalTA4-cryaa:Citrine* plasmid, previously linearized with EcoRI/XbaI. The *hsp70l* promoter was amplified from *hsp70l:mCherry-2A-wnt2* (Poulain and Ober, 2011) using primers 613 and 614, cut with ClaI/NsiI, and subsequently cloned into *I-SceI-phiC31 integrase* cut with the same enzymes. Primers 86, 382, 347 were used for sequencing the *I-SceI-hsp70l:phiC31 integrase* plasmid. The *he1a:palm-Citrine* marker cassette was generated by replacing the promoter sequence in the *UASself-cryaa:Citrine* plasmid (Cayuso et al., 2016) with the hatching enzyme 1a (*he1a*) promoter sequence (a kind gift from the R. Koester laboratory, Technical University of Braunschweig, Germany). The *he1a:palm-Citrine-SV40polyA* cassette was amplified with primers 617 and 618, and cloned into I-SceI-phiC31 cut with Acc65I/SwaI, using blunt-end cloning.

hsp70l:phiC31-sfGFP-NLS

The previously described *I-SceI-hsp70l:phiC31-he1a:palm-Citrine* was modified by replacing the stop codon after the *phiC31* sequence with a linker sequence (5′-acttggttccag-3′). The resulting plasmid was called *I-SceI-hsp70l:phiC31-linker-he1a:palm-Citrine*. The *sfGFP* sequence (a kind gift from H. Knaut's laboratory, Skirball Institute of Biomolecular Medicine, NYU, USA) was amplified with primers 628 and 629, and cloned into *I-SceI-hsp70l:phiC31-linker-he1a:palm-Citrine* with PspOMI. Finally, the *NLS* sequence was added in frame at the C-terminal of the CDS by an intermediate subcloning step into *pBSII-BFP-NLS*. The final plasmid *I-SceI-hsp70l:phiC31-sfGFP-NLS-he1p:palm-Citrine* was sequenced with primers 382, 355, 581 and 615.

Transgenesis

fraeppli2.0-nls and *fraeppli2.0-caax* plasmids were injected into one-cell stage embryos together with *tol2* mRNA (30 pg mRNA and 20 pg DNA/embryo) as previously described (Kawakami et al., 2000). Individual F1 *fraeppli* fish were tested for recombination efficiency, using *cre* or *phiC31 integrase* mRNA injection. The three or four best lines are maintained as the stable lines *fraeppli-nls*$^{cph1\text{-}3,cph9}$ and *fraeppli-caax*$^{cph4\text{-}6}$. The *I-SceI-hsp70l:phiC31-he1a:palm-Citrine* and *I-SceI-fabp10a:kalTA4-cryaa:Venus* plasmids were injected in one cell-stage embryos together with I-SceI enzyme (NEB) as previously described (Soroldoni et al., 2009). Stable transgenic insertions are maintained as *hsp70l:phiC31*^{cph7} and *fabp10a:kalTA4*^{cph8}.

FRaeppli activation

To either prime or activate FRaeppli recombination, *cre* mRNA (20-25 pg) or *phiC31 integrase* mRNA (30-40 pg) was injected into one-cell stage embryos, as described previously (Felker and Mosimann, 2016; Mosimann et al., 2013). For temporally controlled activation, *fraeppli* and desired Gal4/KalTA4 driver lines were crossed to either *tg(hsp70l:cre)*^{zdf13} or *tg(hsp70l:phiC31-he1a:palm-Citrine)*^{cph7}. Embryos were subjected to a 30-60 min heat-shock at 39°C and selected for recombination at desired stages. The recombination in Cre-primed embryos follows the sequential onset of transgenic Gal4/KalTA4 and subsequent FRaeppli-inbuilt PhiC31 integrase expression.

HCR analysis

mRNA expression of *hsp70l:phiC31* was analysed by *in situ* Hybridization Chain Reaction (HCR) RNA FISH version 3.0 (Choi et al., 2018). HCR probes against PhiC31 were purchased from Molecular Instruments. Fixation, detection and amplification were performed according to the HCR v3.0 protocol for whole-mount zebrafish larvae (Choi et al., 2016), apart from the following modifications: 1 pmol of the probe set were used for detection and only 15 pmol hairpin solutions were used for signal amplification. Samples were counterstained with 1:500 DAPI overnight at 4°C. Embryos were mounted in Vectashield and imaged with a Zeiss 880 confocal microscope using a 40× oil objective. Maximum intensity projections of *z*-stacks were generated in Imaris and representative images are shown in the figures.

Imaging

Embryos and larvae intended for imaging experiments were raised in E3 medium (5 mM NaCl, 0.17 mM KCl, 0.33 mM $CaCl_2$ and 0.33 mM $MgSO_4$) supplemented with 0.2 mM 1-phenyl 2-thiourea (PTU, Sigma-Aldrich) to inhibit pigmentation. For live imaging, embryos and larvae were embedded in 0.8% low melting agarose and anesthetized with Tricaine (164 mg/l; MS-222, Sigma-Aldrich) dissolved in E3/PTU. For the time series in Fig. 4, four embryos were selected for three or four colour clones and mounted in a single plate for concurrent imaging every 12-15 min for 8-12 h using sequential acquisition parameters (Fig. S4A). Stained larvae were embedded in VectaShield (Vector labs) for whole-mount imaging. Whole liver lobes or vibratome sections of adult livers were cleared and imaged in SeeDB2S or embedded and imaged in VectaShield. Imaging was performed on Zeiss LSM 780, 880 and 980 confocal microscopes equipped with PMT detectors for sequential imaging and a spectral detector (GaAsP-PMT, 32 channels, 410-694 nm range, 8.9 nm bandwidth) for spectral acquisition. Five-colour sequential imaging was performed with a Leica Stellaris confocal microscope equipped with a tunable white-light laser and four PMT/HyD detectors. In spectral acquisitions, all four FRaeppli FPs were simultaneously excited with 405 nm, 456 nm and 561 nm lasers. In sequential acquisition experiments, 515 nm and 594 nm excitation lasers were needed to discriminate between mOrange2/E2-Orange and mKate2. Additional FPs or fluorophores were excited with a 488 nm and a 633 nm

Development (2022) 149, dev199615. doi:10.1242/dev.199615

laser. Details of imaging parameters for different microscope set-ups are described in Fig. S4A.

Immunostaining

Embryos were fixed with 4% PFA at 4°C overnight and stained as previously described (Thestrup et al., 2019). Adult fish were fixed overnight in 4% PFA at 4°C, using a rotator. Livers of adult fish were dissected, embedded in 4% agarose/water, cut into 130 µm sections using a vibratome (Leica) and stained using the desired antibodies. Alternatively, dissected liver lobes were stained as whole-mount and subsequently cleared following the SeeDB2S protocol (Ke et al., 2016). The following primary and secondary antibodies were used: α-2F11 (mouse monoclonal, 1:10,000, a gift from Julian Lewis, CRUK London Research Institute, UK), anti-MDR1 (rabbit polyclonal antibody, 1:2000, Santa Cruz Biotechnology, sc-8313), goat anti-mouse 488 (1:500, Jackson Immunoresearch) and goat anti-rabbit 647 (1:500, Jackson Immunoresearch). Fixed embryos and adult liver lobes were incubated in 0.1% PBS-Triton X, Alexa Fluor 488 phalloidin (1:1000, Molecular Probes, A12379) and TO-PRO-3 stain (1:50,000, Thermo Fisher Scientific) for 1 h at room temperature or overnight at 4°C. Fresh samples were used for staining and imaging, as FRaeppli endogenous fluorescence is stable in fixed tissue for at least 1-2 weeks.

Image analysis

Images were processed with Bitplane Imaris and Zeiss ZEN software. Maximum intensity projections of *z*-plane stacks are shown, unless indicated differently in the figure legends. For FRaeppli CAAX images, the gamma value of each FRaeppli channel was increased to 1.2-1.5 to better visualize dark regions of the cell membranes. The gamma value was not altered for analysis purposes.

Colour unmixing

Lambda scans were spectrally unmixed using Hyper-Spectral Phasor software (HySP) (version 0.9.10) (Cutrale et al., 2017) (https://bioimaging.usc.edu/software.html). 16-bit spectral images stored in lsm5 format were opened in HySP with harmonic number 1. Images were de-noised in the phasor window to reduce spectral scattering by 10-fold filtering. The minimum intensity values were manually adjusted to subtract dark background, and the phasor was displayed in logarithmic scale. Different clusters in the phasor plot corresponding to the spectra of the fluorescent proteins were manually gated using the polygon ROI selector (see Fig. 3A′) following the Detailed Guide to HySP (https://bioimaging.usc.edu/software.html#instructions). The overlap of the ROI in the image window was used to verify the ROI positions.

Of note, for *fraeppli-caax* we recommend comparing the sequential and spectral acquisition for any given experiment, as faithful colour assignment at cell interfaces of touching cells using the hyperspectral phasor plot is more complex. This also depends on the labelling density obtained. The most reliable, though slower, option is to use sequential acquisition settings. This does not apply to *fraeppli-nls* acquisitions as nuclear signals never spatially intersect.

Quantification of colour distribution

To quantify colour choice in *fraeppli-caax*, embryos of the genotype *fraeppli-caax*^{cph4}*; prox1a:kalTA4*^{uq3bh}*; hsp70l:cre*^{zdf13} were either injected with *cre* mRNA at the one-cell stage or *hsp70l:cre* expression was induced at 33 hpf. Stacks of the first 30 µm of liver tissue were acquired by live imaging with spectral acquisition at 5 dpf, followed by manual annotation of the recombined cells in the Zeiss ZEN software. Embryos of genotype *fraeppli-nls*^{cph1}*; prox1a:KalTA4*^{uq3bh}; *hsp:phiC31*^{cph7} were used to quantify colour choice in *fraeppli-nls*. Recombination was induced by heat shock at 36 hpf as described above. The left liver lobe of 5 dpf larvae was acquired live by spectral imaging. Sequential HySP unmixing was followed by segmentation in Imaris and determination of the number of nuclei using the Spots function.

Quantification of FRaeppli transgene recombination

DNA was extracted from single embryos of the indicated genotypes (Fig. S3F,G). PCRs amplifying recombined transgene species or un-recombined controls were performed (strategy in Fig. S3E). The following primers were used: 666 and 667 (a; detecting a common region in the transgene), 170-662 (b; detecting TagBFP in recombined transgene), 170-346 (c; detecting mTFP1 in recombined transgene), 170-663 (d; detecting mOrange2 in recombined transgene) and 170-664 (e; detecting mKate2 in recombined transgene). The same PCR reactions were performed on 10 ng of FRaeppli 1.0 and 2.0 plasmid as control templates, as FRaeppli 1.0 recombines randomly during *E. coli* growth and thereby was used as positive control of recombination (see 'Constructs' section). Pictures of agarose gels were taken with different exposure times depending on the PCR, to avoid overexposing bands. Band quantification was performed with GelAnalyzer 19.1 (www.gelanalyzer.com; by Istvan Lazar, Jr and Istvan Lazar, Sr), using a morphometric algorithm to automatically define the background. Each band for the recombined versions (b,c) was first normalized to the intensity of the common band (a) from the same sample to correct for differences in DNA content. A second normalization factor for correcting the differences in picture exposure time was then calculated by measuring the 1000 bp band of the ladder (GeneRuler 100 bp plus, Thermo Fisher Scientific) in each picture and applied to each band. Finally, the PCR efficiency, for detecting each recombined colour, was calculated by comparing the normalized intensities of the bands (b-e) of the positive control (FRaeppli 1.0 construct). The PCR efficiency normalization factor for each colour was then applied to every experimental band of the corresponding colour.

For comparison of recombination efficiency in independent *fraeppli-caax* and *fraeppli-nls* lines (Fig. S2D,E), stacks of the first 100 µm of liver tissue were imaged live with spectral acquisition at 5 dpf, followed by manual cluster annotation. In this context, adjacent labelled cells were considered as clusters.

Analysis of hepatocyte canaliculus topology

In 5 dpf stained larvae, FRaeppli FPs were imaged with spectral acquisition and the MDR-stained canaliculi (Alexa 488) in a separate acquisition with a PMT detector, as only a weak signal was detected in the spectral image. The spectral image was processed with the hyperspectral phasor software (see above) and seven channels were identified: four FRaeppli colours (B, C, Y and R) and the intersecting channels between Tag-BFP and mTFP1 (B/C), between mTFP1 and MDR (C/MDR), and between mOrange2 and MDR (Y/MDR). The intersecting channels were used in the analysis to correctly assign pixels that were positive for two adjacent colours in the spectrum, indicating spatial colocalization. The optimized unmixing gates were applied to all images and minimally adjusted to include all significant pixels in each image.

Segmentation was performed in Imaris. First, the seven unmixed channels (exported from the Phasor software) and the MDR channel of each image were combined in a single file in Imaris, following the application of a 5×5×5 median filter to the MDR channel. Subsequently, all the eight channels (cell membranes and canaliculi) were segmented in 3D with the 'Surface' function. An additional surface was created by merging the surfaces of the seven FRaeppli channels (cell membranes). The merged surface was used to select a subset of canaliculi overlapping FRaeppli-labelled cells, by intersecting the two surfaces (FRaeppli membranes and canaliculi). The individual surfaces of the segmented membranes were subsequently used to create masked channels, whereby each colour-positive pixel was set to the same maximal value by thresholding (each included pixel=1; each excluded pixel=0). By doing this, intensity quantifications for each masked channel would also translate in relative volume estimation. For each FRaeppli-positive segmented canaliculus, several parameters were exported for further analysis: the Intensity Mean of each masked channel, indicating the relative volume of each canaliculus that was positive for that colour, the Shortest distance to Surface, indicating all the reciprocal distances between the canaliculi, and the Sphericity.

All parameters were imported into a custom-made script coded in R (RStudio Team, 2019; R Core Team, 2020) to extract the topological information for all analysed canaliculi. First, each canaliculus was associated with one or multiple colours, using a 5% threshold of pixel occupancy for each channel, and the intersecting channels as quality controls. Second, the sphericity (<0.75) and distance (<0.5 µm) between

Development (2022) 149, dev199615. doi:10.1242/dev.199615

each canaliculus were used to classify canaliculi with an 'acinar' configuration, namely those shared between neighbouring hepatocytes that also contain an intracellular region (Fig. 4A). Acinar canaliculi with >30% of pixels occupied by one or multiple colours were considered in the final classification.

A threshold of total colour occupancy of >70% was applied for all the remaining canaliculi, which were subsequently divided into 'intracellular' or 'shared' according to the presence of one or multiple colours, respectively. An additional distance filter was applied to exclude intracellular canaliculi of neighbouring cells of the same colour in a 14 µm radius, which is the typical size of a hepatocyte, as shared or intracellular configurations cannot be discriminated in those cases. Thereby, only canaliculi included in isolated cells or cells surrounded by neighbours of different colours were included in the final classification.

Statistics and reproducibility

Statistical analysis was performed with GraphPad Prism (version 9.3.1). Statistical significance was calculated using the two-tailed Student's *t*-test; n.s. $P \geq 0.05$. All data are presented as mean±s.d. Unless indicated otherwise, *n* refers to sample size (e.g. individual embryos) and *N* refers to biological replicates. For adult tissue stainings, at least three sections were analysed for each biological replicate.

Acknowledgements

We apologise to colleagues whose primary work was not included due to space constraints. We thank E. Caussinus and M. Affolter for sharing the Raeppli constructs; X. Guo for key cloning advice; R. Heyne for cloning of *fabp10a:kalTA4*; E. Ambrosio Galindo for help with processing of adult tissue; O. Andersson, W. Herzog, K. Koltowska, B. Hogan, C. Mosimann, D. Stainier and D. Wilkinson for additional constructs and zebrafish lines; and M. Walther and K. Kristiansen in Zürich and the department of experimental medicine (AEM) in Copenhagen for expert fish care. We gratefully acknowledge the DanStem Imaging Platform (University of Copenhagen), the Translational Imaging Center (University of Southern California), the ScopeM (ETH-Zurich), and the Center for Microscopy and Image Analysis (University of Zurich) for their support and assistance in this work.

Competing interests

F.C. and S.E.F. have intellectual property rights in the area of hyperspectral imaging and they are co-founders of Kulia Laboratories, a company that is advancing hyperspectral imaging.

Author contributions

Conceptualization: S.C., E.A.O.; Methodology: S.C., I.A.U., A.G., A.E.V.; Software: A.G., F.C., L.A.T., S.E.F.; Validation: S.C., I.A.U.; Formal analysis: S.C., I.A.U., A.G.; Resources: F.C., L.A.T., S.E.F., S.C.F.N., E.A.O.; Writing - original draft: S.C., I.A.U., E.A.O.; Writing - review & editing: S.C., I.A.U., A.G., F.C., L.A.T., S.E.F., S.C.F.N., E.A.O.; Visualization: S.C., I.A.U.; Supervision: E.A.O.; Funding acquisition: E.A.O.

Funding

The Novo Nordisk Center for Stem Cell Biology is supported by the Novo Nordisk Fonden (NNF17CC0027852). This work was further supported by the Danmarks Grundforskningsfond (DNRF116). S.C. was supported by a Schweizerischer Nationalfonds zur Förderung der Wissenschaftlichen Forschung Early Postdoc Mobility fellowship (P2ZHP3_164840), by a Long Term European Molecular Biology Organization Postdoc fellowship (ALTF 511-2016) and by a Suslowa fellowship from the Universität Zürich. Work in S.C.F.N.'s laboratory was supported by the by the Schweizerischer Nationalfonds zur Förderung der Wissenschaftlichen Forschung (31003A_173083 and 310030_200376). F.C., L.A.T. and S.E.F. were supported by the University of Southern California and the Alfred E. Mann Institute for Biomedical Engineering, University of Southern California.

References

Bischof, J., Maeda, R. K., Hediger, M., Karch, F. and Basler, K. (2007). An optimized transgenesis system for Drosophila using germ-line-specific phiC31 integrases. *Proc. Natl. Acad. Sci. USA* **104**, 3312-3317. doi:10.1073/pnas.0611511104

Brand, A. H. and Perrimon, N. (1993). Targeted gene expression as a means of altering cell fates and generating dominant phenotypes. *Development* **118**, 401-415. doi:10.1242/dev.118.2.401

Carney, T. J. and Mosimann, C. (2018). Switch and trace: recombinase genetics in Zebrafish. *Trends Genet.* **34**, 362-378. doi:10.1016/j.tig.2018.01.004

Caviglia, S. and Ober, E. A. (2018). Non-conventional protrusions: the diversity of cell interactions at short and long distance. *Curr. Opin. Cell Biol.* **54**, 106-113. doi:10.1016/j.ceb.2018.05.013

Cayuso, J., Dzementsei, A., Fischer, J. C., Karemore, G., Caviglia, S., Bartholdson, J., Wright, G. J. and Ober, E. A. (2016). EphrinB1/EphB3b coordinate bidirectional epithelial-mesenchymal interactions controlling liver morphogenesis and laterality. *Dev. Cell* **39**, 316-328. doi:10.1016/j.devcel.2016.10.009

Chan, K. Y., Yan, C.-C. S., Roan, H.-Y., Hsu, S.-C., Tseng, T.-L., Hsiao, C.-D., Hsu, C.-P. and Chen, C.-H. (2022). Skin cells undergo asynthetic fission to expand body surfaces in zebrafish. *Nature* **605**, 119-125. doi:10.1038/s41586-022-04641-0

Choi, H. M. T., Calvert, C. R., Husain, N., Huss, D., Barsi, J. C., Deverman, B. E., Hunter, R. C., Kato, M., Lee, S. M., Abelin, A. C. et al. (2016). Mapping a multiplexed zoo of mRNA expression. *Development* **143**, 3632-3637. doi:10.1242/dev.140137

Choi, H. M. T., Schwarzkopf, M., Fornace, M. E., Acharya, A., Artavanis, G., Stegmaier, J., Cunha, A. and Pierce, N. A. (2018). Third-generation in situ hybridization chain reaction: multiplexed, quantitative, sensitive, versatile, robust. *Development* **145**, dev165753. doi:10.1242/dev.165753

Clerbaux, L.-A., Manco, R., Van Hul, N., Bouzin, C., Sciarra, A., Sempoux, C., Theise, N. D. and Leclercq, I. A. (2019). Invasive ductular reaction operates hepatobiliary junctions upon hepatocellular injury in rodents and humans. *Am. J. Pathol.* **189**, 1569-1581. doi:10.1016/j.ajpath.2019.04.011

Cook, Z. T., Brockway, N. L., Tobias, Z. J. C., Pajarla, J., Boardman, I. S., Ippolito, H., Nkombo Nkoula, S. and Weissman, T. A. (2019). Combining near-infrared fluorescence with Brainbow to visualize expression of specific genes within a multicolor context. *Mol. Biol. Cell* **30**, 491-505. doi:10.1091/mbc.E18-06-0340

Cutrale, F., Trivedi, V., Trinh, L. A., Chiu, C.-L., Choi, J. M., Artiga, M. S. and Fraser, S. E. (2017). Hyperspectral phasor analysis enables multiplexed 5D in vivo imaging. *Nat. Methods* **14**, 149-152. doi:10.1038/nmeth.4134

Dickinson, M. E., Bearman, G., Tille, S., Lansford, R. and Fraser, S. E. (2001). Multi-spectral imaging and linear unmixing add a whole new dimension to laser scanning fluorescence microscopy. *BioTechniques* **31**, 1272, 1274-1276, 1278. doi:10.2144/01316bt01

Distel, M., Wullimann, M. F. and Köster, R. W. (2009). Optimized Gal4 genetics for permanent gene expression mapping in zebrafish. *Proc. Natl. Acad. Sci. USA* **106**, 13365-13370. doi:10.1073/pnas.0903060106

Felker, A. and Mosimann, C. (2016). Contemporary zebrafish transgenesis with Tol2 and application for Cre/lox recombination experiments. *Methods Cell Biol.* **135**, 219-244. doi:10.1016/bs.mcb.2016.01.009

Feng, H., Langenau, D. M., Madge, J. A., Quinkertz, A., Gutierrez, A., Neuberg, D. S., Kanki, J. P. and Look, A. T. (2007). Heat-shock induction of T-cell lymphoma/leukaemia in conditional Cre/lox-regulated transgenic zebrafish. *Br. J. Haematol.* **138**, 169-175. doi:10.1111/j.1365-2141.2007.06625.x

Fontenas, L. and Kucenas, S. (2021). Spinal cord precursors utilize neural crest cell mechanisms to generate hybrid peripheral myelinating glia. *eLife* **10**, e64267. doi:10.7554/eLife.64267

Förster, D., Dal Maschio, M., Laurell, E. and Baier, H. (2017). An optogenetic toolbox for unbiased discovery of functionally connected cells in neural circuits. *Nat. Commun.* **8**, 116. doi:10.1038/s41467-017-00160-z

Gupta, V. and Poss, K. D. (2012). Clonally dominant cardiomyocytes direct heart morphogenesis. *Nature* **484**, 479-484. doi:10.1038/nature11045

Gurevich, D. B., Nguyen, P. D., Siegel, A. L., Ehrlich, O. V., Sonntag, C., Phan, J. M. N., Berger, S., Ratnayake, D., Hersey, L., Berger, J. et al. (2016). Asymmetric division of clonal muscle stem cells coordinates muscle regeneration in vivo. *Science* **353**, aad9969. doi:10.1126/science.aad9969

Her, G. M., Yeh, Y.-H. and Wu, J.-L. (2003). 435-bp liver regulatory sequence in the liver fatty acid binding protein (L-FABP) gene is sufficient to modulate liver regional expression in transgenic zebrafish. *Dev. Dyn.* **227**, 347-356. doi:10.1002/dvdy.10324

Hu, G., Goll, M. G. and Fisher, S. (2011). PhiC31 integrase mediates efficient cassette exchange in the zebrafish germline. *Dev. Dyn.* **240**, 2101-2107. doi:10.1002/dvdy.22699

Jin, S.-W., Beis, D., Mitchell, T., Chen, J.-N. and Stainier, D. Y. R. (2005). Cellular and molecular analyses of vascular tube and lumen formation in zebrafish. *Development* **132**, 5199-5209. doi:10.1242/dev.02087

Kamimoto, K., Nakano, Y., Kaneko, K., Miyajima, A. and Itoh, T. (2020). Multidimensional imaging of liver injury repair in mice reveals fundamental role of the ductular reaction. *Commun Biol* **3**, 289. doi:10.1038/s42003-020-1006-1

Kanca, O., Caussinus, E., Denes, A. S., Percival-Smith, A. and Affolter, M. (2014). Raeppli: a whole-tissue labeling tool for live imaging of Drosophila development. *Development* **141**, 472-480. doi:10.1242/dev.102913

Kawakami, K., Shima, A. and Kawakami, N. (2000). Identification of a functional transposase of the Tol2 element, an Ac-like element from the Japanese medaka fish, and its transposition in the zebrafish germ lineage. *Proc. Natl. Acad. Sci. USA* **97**, 11403-11408. doi:10.1073/pnas.97.21.11403

Ke, M. T., Nakai, Y., Fujimoto, S., Takayama, R., Yoshida, S., Kitajima, T. S., Sato, M. and Imai, T. (2016). Super-resolution mapping of neuronal circuitry with

an index-optimized clearing agent. *Cell Rep.* **14**, 2718-2732. doi:10.1016/j.celrep.2016.02.057

Koltowska, K., Lagendijk, A. K., Pichol-Thievend, C., Fischer, J. C., Francois, M., Ober, E. A., Yap, A. S. and Hogan, B. M. (2015). Vegfc regulates bipotential precursor division and prox1 expression to promote lymphatic identity in zebrafish. *Cell Rep.* **13**, 1828-1841. doi:10.1016/j.celrep.2015.10.055

Lister, J. A. (2011). Use of phage phiC31 integrase as a tool for zebrafish genome manipulation. *Methods Cell Biol.* **104**, 195-208. doi:10.1016/B978-0-12-374814-0.00011-2

Livet, J., Weissman, T. A., Kang, H., Draft, R. W., Lu, J., Bennis, R. A., Sanes, J. R. and Lichtman, J. W. (2007). Transgenic strategies for combinatorial expression of fluorescent proteins in the nervous system. *Nature* **450**, 56-62. doi:10.1038/nature06293

Lorent, K., Yeo, S.-Y., Oda, T., Chandrasekharappa, S., Chitnis, A., Matthews, R. P. and Pack, M. (2004). Inhibition of Jagged-mediated Notch signaling disrupts zebrafish biliary development and generates multi-organ defects compatible with an Alagille syndrome phenocopy. *Development* **131**, 5753-5766. doi:10.1242/dev.01411

Megason, S. G. and Fraser, S. E. (2007). Imaging in systems biology. *Cell* **130**, 784-795. doi:10.1016/j.cell.2007.08.031

Mosimann, C., Puller, A. C., Lawson, K. L., Tschopp, P., Amsterdam, A. and Zon, L. I. (2013). Site-directed zebrafish transgenesis into single landing sites with the phiC31 integrase system. *Dev. Dyn.* **242**, 949-963. doi:10.1002/dvdy.23989

Ni, T. T., Lu, J., Zhu, M., Maddison, L. A., Boyd, K. L., Huskey, L., Ju, B., Hesselson, D., Zhong, T. P., Page-McCaw, P. S. et al. (2012). Conditional control of gene function by an invertible gene trap in zebrafish. *Proc. Natl. Acad. Sci. USA* **109**, 15389-15394. doi:10.1073/pnas.1206131109

Pan, Y. A., Freundlich, T., Weissman, T. A., Schoppik, D., Wang, X. C., Zimmerman, S., Ciruna, B., Sanes, J. R., Lichtman, J. W. and Schier, A. F. (2013). Zebrabow: multispectral cell labeling for cell tracing and lineage analysis in zebrafish. *Development* **140**, 2835-2846. doi:10.1242/dev.094631

Parsons, M. J., Pisharath, H., Yusuff, S., Moore, J. C., Siekmann, A. F., Lawson, N. and Leach, S. D. (2009). Notch-responsive cells initiate the secondary transition in larval zebrafish pancreas. *Mech. Dev.* **126**, 898-912. doi:10.1016/j.mod.2009.07.002

Poulain, M. and Ober, E. A. (2011). Interplay between Wnt2 and Wnt2bb controls multiple steps of early foregut-derived organ development. *Development* **138**, 3557-3568. doi:10.1242/dev.055921

R Core Team. (2020). *R: A Language and Environment for Statistical Computing*. Vienna, Austria: R Foundation for Statistical Computing.

Reddy, V. B., Ghosh, P. K., Lebowitz, P., Piatak, M. and Weissman, S. M. (1979). Simian virus 40 early mRNA's. I. Genomic localization of 3′ and 5′ termini and two major splices in mRNA from transformed and lytically infected cells. *J. Virol.* 30, 279-296. doi:10.1128/jvi.30.1.279-296.1979

Richier, B. and Salecker, I. (2015). Versatile genetic paintbrushes: Brainbow technologies. *Wiley Interdiscip Rev Dev Biol* **4**, 161-180. doi:10.1002/wdev.166

RStudio Team. (2019). *RStudio: Integrated Development for R*. Boston, MA: RStudio, Inc.

Rulands, S. and Simons, B. D. (2016). Tracing cellular dynamics in tissue development, maintenance and disease. *Curr. Opin. Cell Biol.* **43**, 38-45. doi:10.1016/j.ceb.2016.07.001

Rupp, R. A., Snider, L. and Weintraub, H. (1994). Xenopus embryos regulate the nuclear localization of XMyoD. *Genes Dev.* **8**, 1311-1323. doi:10.1101/gad.8.11.1311

Sakaguchi, T. F., Sadler, K. C., Crosnier, C. and Stainier, D. Y. R. (2008). Endothelial signals modulate hepatocyte apicobasal polarization in zebrafish. *Curr. Biol.* **18**, 1565-1571. doi:10.1016/j.cub.2008.08.065

Sanders, T. A., Llagostera, E. and Barna, M. (2013). Specialized filopodia direct long-range transport of SHH during vertebrate tissue patterning. *Nature* **497**, 628-632. doi:10.1038/nature12157

Soroldoni, D., Hogan, B. M. and Oates, A. C. (2009). Simple and efficient transgenesis with meganuclease constructs in zebrafish. *Methods Mol. Biol.* **546**, 117-130. doi:10.1007/978-1-60327-977-2_8

Thestrup, M. I., Caviglia, S., Cayuso, J., Heyne, R. L. S., Ahmad, R., Hofmeister, W., Satriano, L., Wilkinson, D. G., Andersen, J. B. and Ober, E. A. (2019). A morphogenetic EphB/EphrinB code controls hepatopancreatic duct formation. *Nat. Commun.* **10**, 5220. doi:10.1038/s41467-019-13149-7

Thorpe, H. M., Wilson, S. E. and Smith, M. C. M. (2000). Control of directionality in the site-specific recombination system of the Streptomyces phage phiC31. *Mol. Microbiol.* **38**, 232-241. doi:10.1046/j.1365-2958.2000.02142.x

Treyer, A. and Müsch, A. (2013). Hepatocyte polarity. *Comp. Physiol.* **3**, 243-287. doi:10.1002/cphy.c120009

Urasaki, A., Morvan, G. and Kawakami, K. (2006). Functional dissection of the Tol2 transposable element identified the minimal cis-sequence and a highly repetitive sequence in the subterminal region essential for transposition. *Genetics* **174**, 639-649. doi:10.1534/genetics.106.060244

Weissman, T. A. and Pan, Y. A. (2015). Brainbow: new resources and emerging biological applications for multicolor genetic labeling and analysis. *Genetics* **199**, 293-306. doi:10.1534/genetics.114.172510

Westerfield, M. (2000). *The Zebrafish Book: A Guide for the Laboratory Use of Zebrafish (Danio rerio)*. Eugene, OR: University of Oregon Press.